ADVANCED SUSTAINABLE SYSTEMS

www.advsustainsys.com

# Graphene–Perovskite Schottky Barrier Solar Cells

*Yi Song, Anna Osherov, Vladimir Bulović, and Jing Kong**

**Perovskite solar cells have attained incredible power conversion efficiencies but it is still unclear whether photogenerated carriers are free or excitonic in nature. Originally, it is believed that they are exciton-based devices, similar to organic or dye-sensitized solar cells. However, the emergence of efficient planar devices as well as measurements of exciton binding energy in the range of 10–100 meV suggest that they may be free carrier-based. In this work, the free carrier model is confirmed by building graphene/perovskite Schottky barrier solar cells, analogous to conventional metal/semiconductor Schottky barrier solar cells. To address the challenges of building such devices, solution-processing techniques are extensively investigated for depositing perovskite films directly onto graphene in order to obtain an intimate contact between the graphene and perovskite. Interestingly, these graphene/perovskite Schottky barrier devices have reasonably good efficiency—up to 10.6%—and short circuit current densities only slightly lower than control devices. Furthermore, devices with neither a hole transport layer nor an electron transport layers have power conversion efficiencies of up to 6%. These results provide convincing evidence supporting the free carrier model for methylammonium lead iodide perovskites and offer insights on potential alternative designs for perovskite solar cells.**

## 1. Introduction

Perovskite solar cells have attained power conversion efficiencies (PCEs) of over 22% in recent years. The potential for low-cost solution processed devices combined with high efficiencies compared to other emerging technologies has attracted significant attention from researchers. However, fundamental questions regarding the photovoltaic mechanism of these devices remain unanswered. In particular, it is still unclear whether photogenerated electron–hole pairs behave as free carriers or exictons. Originally, it was believed that perovskite solar cells were exciton-based devices, similar to organic or dye-sensitized solar cells, whereby a heterojunction is needed to dissociate tightly bound electron–hole pairs. In accordance with this understanding, the first perovskite solar cells demonstrated in laboratories involved coating the $CH_3NH_3PbI_3$ film onto a mesoporous titanium oxide scaffold and using a liquid electrolyte.[1] However, more recently, researchers have demonstrated efficient planar heterojunction devices for both standard (e.g., indium tin oxide (ITO)/$TiO_x$/$CH_3NH_3PbI_3$/Spiro/Au) and inverted (ITO/poly(3,4-ethylenedioxythiophene) (PEDOT):polystyrene sulfonate (PSS)/$CH_3NH_3PbI_3$/fullerene derivative: [6,6]-phenyl-$C_{61}$-butyric acid methyl ester (PCBM)/Al) topologies.[2] Some of these topologies have also been shown to function without a hole transport layer (HTL) or electron transport layer (ETL), for example, by depositing the perovskite film directly onto ITO or fluorine doped tin oxide.[3] Furthermore, several works measured the excitonic binding energy in perovskite films to be in the order of 10–100 meV, which suggests that indeed many or most excitons are dissociated into electron–hole pairs at room temperature.[4] These results suggest that perovskite devices may be free carrier-based, whereby photogenerated electron–hole pairs dissociate quickly and are free to move independently. Thus, it is possible that perovskites are more similar to conventional semiconductor photovoltaic materials such as silicon. To further explore this idea, we build Schottky barrier-based perovskite solar cells, where the perovskite is placed in direct contact with a metal of appropriate work function. This type of device structure relies on a built-in electric field to separate electron–hole pairs and should therefore only work if charge carriers in perovskite films are free or loosely bound. If, on the other hand, electron–hole pairs are tightly bound, the charge-neutral excitons will not be affected by the electric field and will likely be quenched at the perovskite/metal interface. Thus, the performance of this device structure will shed further light on the nature of charge carriers in perovskite solar cells.

Conventional bulk semiconductors such as silicon or gallium arsenide (GaAs) can be used to build Schottky barrier solar cells by putting a metal in contact with the semiconductor. This mismatch in work function between the metal and semiconductor produces a built-in electric field, which separates photogenerated electron–hole pairs. Advantages of semiconductor–metal Schottky barrier solar cells over their p–n heterojunction counterparts include simplicity and lower processing temperatures because a diffusion step is not necessary. However, the PCE is typically lower than that of heterojunction devices.[5] Part of the difficulty in designing Schottky barrier devices lies in finding a compatible metal with appropriate work function to achieve the highest possible Schottky barrier height. Perovskite films are typically n-doped, which require a high work function metal such as gold or silver to form a Schottky barrier.[6] In practice, there are several key

Dr. Y. Song, Dr. A. Osherov, Prof. V. Bulović, Prof. J. Kong
Department of Electrical Engineering and Computer Sciences
Massachusetts Institute of Technology
Cambridge, MA 02139, USA
E-mail: jingkong@mit.edu

DOI: 10.1002/adsu.201700106

 

challenges in fabricating such a device. Because metals are not transparent, they must be patterned into a grid in order to allow light to pass into the active layer. The required pitch of the grid is determined approximately by carrier diffusion lengths in the active material. In triiodide perovskites, diffusion lengths are typically in the order of 100 nm – 1 μm, compared to tens or hundreds of microns in silicon, which makes the required grid pitch difficult to achieve with shadow masks.[7] Moreover, it has been shown that gold can migrate into perovskite layers and that the iodine in perovskites react with silver.[8] These issues were observed even though an HTL was present between the metal and perovskite and are therefore likely to be exacerbated if the metal is in direct contact with the perovskite.

Here, we choose graphene as the metal for forming the Schottky barrier with the perovskite because it has several key advantages that help overcome the challenges discussed above. Graphene has been investigated as a potential alternative transparent conductor in numerous photovoltaic technologies, include perovskite solar cells.[9] First, graphene is thin enough to be optically transparent so it does not need to be patterned into a grid. Also, graphene is chemically inert and should not react with perovskite films. Furthermore, the work function of graphene can be tuned via chemical doping; heavy p-doping can raise the work function of graphene to be nearly as high as that of gold,[10] allowing it form a high Schottky barrier with perovskite films. Graphene/silicon and graphene/GaAs Schottky barrier solar cells have been demonstrated, achieving PCE's of 15% and 18%, respectively.[11] Previously, reduced graphene oxide was used by Yan et al. to form a Schottky junction with perovskite.[12] Here, we use graphene synthesized via chemical vapor deposition (CVD) because it offers better conductivity and uniformity. The particular Schottky device structure we study in this work is graphene/$CH_3NH_3PbI_3$/PCBM/Ca/Al (**Figure 1**a). In this case, the monolayer CVD graphene, having relatively high carrier density and zero bandgap, behaves as a metal and the perovskite layer is the semiconductor, thereby forming a Schottky junction, as shown in the energy band alignment diagram in Figure 1b. Like in a conventional Schottky diode, electrons transfer from the perovskite to the graphene, causing band-bending at the interface. Such a structure allows us to evaluate whether a Schottky junction between the graphene and perovskite is sufficient to separate electron–hole pairs (Figure 1b). Other structures investigated for reference are standard ITO control devices (ITO/PEDOT:PSS/$CH_3NH_3PbI_3$/PCBM/Ca/Al) and graphene/PEDOT:PSS control devices (graphene/PEDOT:PSS/$CH_3NH_3PbI_3$/PCBM/Ca/Al).

## 2. Results and Discussion

Although graphene has important advantages, there are still several challenges that impede the fabrication of such a device. Graphene is highly hydrophobic, making it difficult to deposit uniform films via spin-coating from polar solvents (such as water). Unfortunately, the most common solvents used in perovskite precursor solutions, such as dimethylformamide (DMF) or dimethyl sulfoxide, are both polar and therefore do not wet graphene well. In our case, the perovskite precursor solution is made using lead acetate ($PbAc_2$) mixed with methylammonium iodide (MAI) in a 1:3 molar ratio dissolved at a concentration of 0.88 M in DMF. Lead acetate is chosen because it produces dense, smooth films and allows for lower annealing temperatures.[2c] ITO/PEDOT:PSS and graphene/PEDOT:PSS control devices were fabricated by dynamically dispensing 35 μL of precursor solution onto a substrate preheated to 85 °C (**Figure 2**a). We find that DMF slowly dissolves PEDOT:PSS so dynamically dispensing the precursor solution minimizes the time the PEDOT:PSS is exposed to DMF. Furthermore, we find that preheating the substrate is critical for achieving the best performance. The coated substrate is then annealed at 85 °C for 15 min to convert the precursors to perovskite. We use this procedure as a starting point for finding the optimum process for devices with bare graphene (i.e., devices without the PEDOT:PSS HTL). However, as expected, dynamically spin-coating the perovskite precursor solution onto graphene (without PEDOT:PSS) results in sparse coverage due to dewetting of the precursor solution (Figure 2b). Furthermore, scanning electron microscope (SEM) examinations reveal that even in regions that are covered, the perovskite film is porous, whereas perovskite films formed on graphene/PEDOT:PSS are dense (Figure 2b). In a Schottky barrier solar cell, photogenerated carriers must be collected by the electrodes in order to contribute to photocurrent. However, the diffusion length of carriers in lead iodide perovskite films is typically in the order of 100 nm.[7] A porous perovskite film will only form a partial contact with the graphene and the photogenerated carriers will need to travel further to reach the graphene electrode. Consequently many

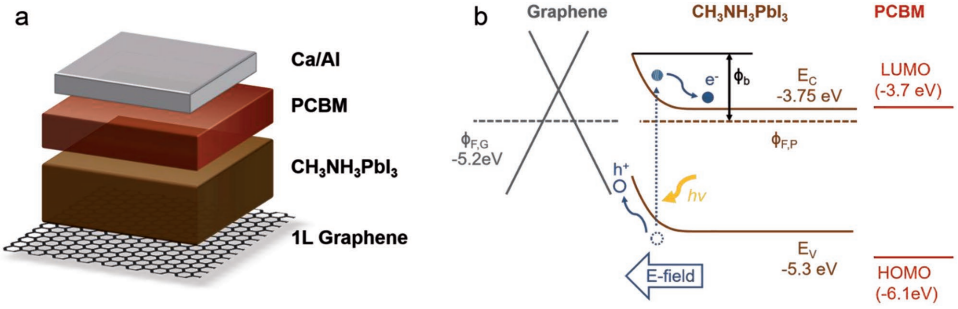


**Figure 1.** a) Structure of graphene/perovskite Schottky barrier solar cell. b) Energy band diagram showing approximate alignment between graphene and perovskite and illustrating the free charge carrier model.

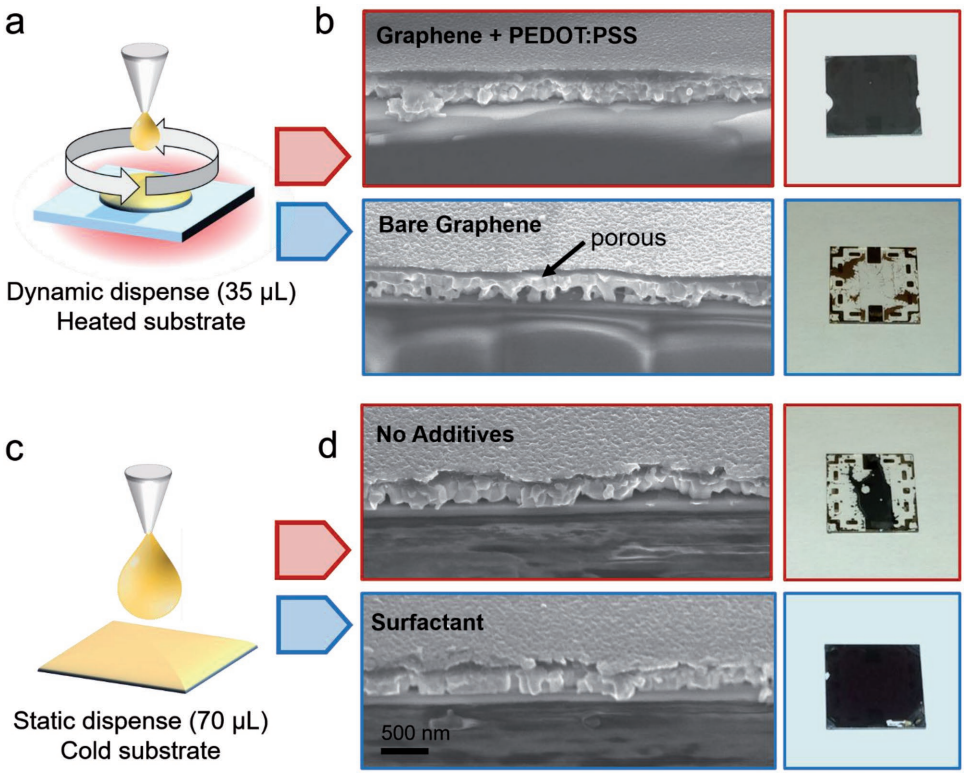


**Figure 2.** a) Schematic of spin-coating process used to achieve optimal performance for control devices. b) SEM and photographs of resultant films deposited onto Graphene/PEDOT:PSS and bare graphene using this procedure. c) Schematic of modified spin-coating procedure and d) SEM and photographs of resultant films deposited using this modified procedure from precursor solutions with and without additives.

carriers will recombine and will not contribute to photocurrent. Based on this understanding, perovskite film porousness should reduce $J_{SC}$ of the device and is therefore expected to be detrimental to performance. Thus, it is necessary to solve both issues (porousness and film coverage) to achieve the best device performance.

In devices with PEDOT:PSS, dynamic spin-coating is necessary to avoid dissolving the PEDOT:PSS. However, since PEDOT:PSS is no longer present in the graphene/perovskite Schottky structure and graphene is resilient to solvents, it is no longer necessary to dynamically dispense the precursor solution. We find that statically dispensing a larger amount (70–100 µL) of precursor solution so that the solution spreads across the entire substrate allows for better coverage (Figure 2c). However, the method is inconsistent and coverage yield is about 70%, which is unsuitable for large-scale production but sufficient for studying device properties. This method is subsequently referred to as a direct spinning.

Additionally, we also evaluate the use of additives to improve wetting. It has been previously reported that adding a small amount of nonionic surfactant to aqueous PEDOT:PSS allows it to be spin-coated uniformly onto graphene.[13] We find that the same technique can be applied to perovskite precursor solution; adding as little as 0.2 wt% of nonionic surfactant allows for consistent uniform coverage. Another possible additive is 1,8-diiodooctane (DiO). DiO has been shown to be effective in improving the performance of organic bulk heterojunction solar cells as well as perovskite solar cells.[14] Here, we find that adding 0.5 wt% DiO into the precursor solution also consistently results in complete coverage (Figure 2d).

In all cases, depositing the precursor onto a heated substrate and immediately annealing results in porous films. However, we find that depositing onto the substrate at room temperature and allowing the film to rest for 2 min before annealing produces denser films for direct spinning and surfactant additives. Unfortunately, films deposited using DiO additive are still porous. From these findings, we suspect that the porosity of perovskite films may result from residual solvent evaporating during the annealing process. Thus, depositing the precursor onto the substrate at room temperature and allowing the film to completely dry before annealing mitigate this issue. DiO has extremely low volatility and is often used to control the morphology of organic bulk heterojunction film in the fabrication of organic solar cells.[15] Thus, it is likely that significant amounts of DiO remain in the film after spinning and resting, which again results in porous films after annealing. These findings related to the deposition of perovskite films directly onto graphene are summarized in Figure 2.

Another challenge is p-doping the graphene to achieve high work function, which is necessary to maximize the Schottky barrier height. A reliable method of substitutional doping has not been found and chemical dopants such as $AuCl_3$ or $HNO_3$ are easily removed when exposed to solvents.[16] Thus, chemically doping the graphene prior to depositing the perovskite film is unlikely to be effective. However, we find that the process of depositing perovskite films onto graphene using

$PbAc_2$ and MAI precursors p-dopes the graphene. The sheet resistance of pristine monolayer graphene films is on glass about 300 Ω per square with sheet carrier concentration of $1.4 \times 10^{13}$ $cm^{-2}$. After spin-coating the precursor solution, the sheet resistance increases to 420 Ω per square, as a result of the carrier concentration decreasing. However, after baking the films at 85 °C for 15 min, the carrier concentration increases to $3.1 \times 10^{13}$ $cm^{-2}$ and the sheet resistance decreases accordingly. This occurs regardless of the method used to spin-coat the perovskite precursor solution (direct spinning or additives). The benefit of this doping is twofold: first, the reduced sheet resistance of the graphene films, resulting in lower series resistance and higher fill factor; second, the doping raises the work function of the graphene and the Schottky barrier height. Equation (1) approximates the Fermi energy relative to the dirac point as a function of doping level. The doping remains stable for at least four months (longest period we have tested thus far) after fabrication if the sample is left inside a nitrogen-filled glove box. The individual chemicals in the precursor solution ($PbAc_2$, MAI, DMF) do not dope the graphene when spin-coated and baked. However, $PbI_2$ does dope graphene. Thus, we believe that the doping results from $PbAc_2$ being converted into $PbI_2$ and released during the perovskite formation process. This would also suggest that the film is composed of $PbAc_2$ and MAI immediately after spinning and is only converted to the perovskite phase after baking. The measured sheet resistance and carrier concentration at different stages in the deposition process are shown in Table S1 in the Supporting Information

$$E_F \approx 11.3\ \text{meV} \cdot \sqrt{\frac{n_s}{10^{10}}} \quad (1)$$

According to Equation (1), the Fermi level of graphene doped at $3.1 \times 10^{13}$ $cm^{-2}$ is 629 meV below the dirac point. Previous literature shows that the energy level of the dirac point in graphene is approximately −4.6 eV, which suggests that the work function of our heavily doped graphene is −5.23 eV. This is higher than the work function of PEDOT:PSS, which is typically reported to be −5.0 eV. We should therefore expect more band bending and, consequently, higher open circuit voltage ($V_{OC}$) in graphene/perovskite devices than ITO/PEDOT:PSS/perovskite devices. This calculation would also suggest that the Schottky barrier height is 1.45 eV if we simply take the barrier height as the difference in electron affinities of the two materials. One peculiarity is that because perovskite is n-doped, we would expect electron transfer from the perovskite to the graphene in forming the depletion region, which should n-dope the graphene. Yet, the graphene is still measured to be heavily p-doped. This apparent inconsistency will be explained later by *C–V* measurements.

The *J/V* characteristics of ITO/PEDOT:PSS, graphene/PEDOT:PSS, and bare graphene devices made using the standard dynamic spin-coating procedure (with porous perovskite films) are shown in **Figure 3**a. The short-circuit current ($J_{SC}$) of devices with porous films on bare graphene is significantly reduced, which is consistent with our understanding that Schottky barrier solar cells require an intimate contact between

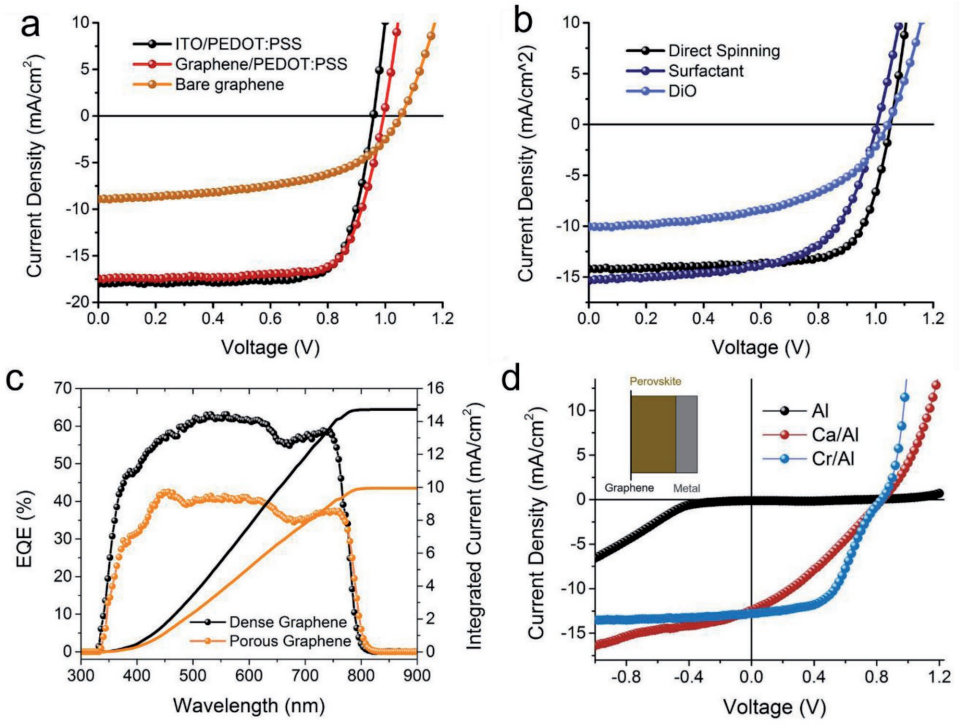


**Figure 3.** a) Comparison of *J/V* characteristics of ITO/PEDOT:PSS, graphene/PEDOT:PSS devices, and graphene device fabricated using dynamic spin-coating onto a heated substrate. b) *J/V* characteristics of graphene/perovskite devices fabricated using direct spinning, surfactant additive, and DiO additive. c) EQE spectra (left axis) and expected current density integrated from EQE spectra (right axis) of dense (direct spinning) and porous (dynamic spinning on heated substrate) perovskite films on graphene. d) *J/V* curves of graphene/perovskite/metal devices.

the metal and the semiconductor. In addition, the fill factor is also poor because the porous morphology inhibits carrier transport from the perovskite into the graphene electrode. However, as expected from our calculation of the work function of graphene, the device on bare graphene has the highest $V_{OC}$ of 1.05 V. In fact, the $V_{OC}$ is even slightly higher than the 0.95 V value reported for graphene/GaAs Schottky barrier devices.[11a] The $J/V$ characteristics of graphene/perovskite Schottky devices made using the optimized spin-coating procedures (statically dispense precursor solution onto cold substrate) are shown in Figure 3b. Devices made by direct spinning without additives show the best performance but have poor yield due to inconsistent coverage. Devices made with surfactant added to the precursor solution have reduced fill factor, likely because of residual surfactant in the film after annealing. Devices made with DiO added to the precursor solution have poor $J_{SC}$ and fill factor because, as mentioned before, the perovskite films are still porous. The difference between devices with dense and porous films is also highlighted by the external quantum efficiency (EQE) spectra, as shown in Figure 3c.

The maximum achieved PCE for graphene/perovskite Schottky devices was 10.6% using direct spinning, which is still somewhat lower than the 13% achieved for ITO/PEDOT:PSS and graphene/PEDOT:PSS devices. The difference in performance is attributed to lower $J_{SC}$ in graphene/perovskite Schottky compared to devices with PEDOT:PSS (≈14.5 mA cm$^{-2}$ vs ≈17.5 mA cm$^{-2}$). This difference indicates that the graphene/perovskite Schottky junction is able to collect about 80–85% as many carriers as a PEDOT:PSS/perovskite junction. Furthermore, it is uncertain whether the reduced $J_{SC}$ is entirely attributed to the quenching of excitons at the graphene/perovskite interface (which suggests that some carriers are still bound). Another possibility is that polymer residue on the graphene causes a partial contact, similar to the case of the porous perovskite films, which will reduce $J_{SC}$, as per the discussion in the previous section. Nonetheless, this strongly suggests that most, but possibly not all, photogenerated carriers in methylammonium lead iodide perovskite films are indeed dissociated. To further evaluate this hypothesis, we also fabricate devices omitting the PCBM electron transport layer (graphene/perovskite/metal). The perovskite film deposited using lead acetate precursor is smooth enough that metal can be directly evaporated onto the perovskite without planarization (typically, the PCBM serves a double role as an ETL and as a planarizing layer). When the PCBM layer is present, the low work function cathode metal forms an Ohmic contact with the PCBM and, ideally, should also form an Ohmic contact with the perovskite film. However, since perovskite films chemically react with metals, the selection of cathode material is critical. Here, we try Al alone, Ca/Al, and Cr/Al. The results are shown in Figure 3d. The Al alone is visibly oxidized by the perovskite film, resulting in very poor performance. The Ca/Al and Cr/Al are not visibly oxidized, but the performance is evidently reduced compared to devices with an ETL. The maximum efficiency achieved is about 6% with the Cr/Al cathode. It is important to note that the reduced performance is attributed to lower $V_{OC}$ and fill factor, not to lower $J_{SC}$. Thus, in agreement with the Schottky barrier model, it is likely that the majority of charge collection takes place at the graphene/perovskite interface. Although the PCE is presently low, these results show that perovskite solar cells can function without a HTL or ETL, which opens up possibilities for alternative device designs in the future.

To further advance our understanding of the graphene/perovskite Schottky junction device, we perform $C–V$ measurements. Typically, in metal–silicon or graphene–silicon Schottky barrier solar cells, the width of the depletion region in silicon decreases with increasing forward bias. As a result, capacitance increases with increasing forward bias. Typical depletion region widths in silicon solar cells range from tens of nanometers to several microns (depending on doping level) while the thickness of the silicon itself is typically several hundred micrometers, so the silicon is unlikely to be completely depleted. However, in the case of perovskite solar cells, the situation is more complicated because thickness of the semiconducting perovskite layer is several hundred nanometers. Thus, if the perovskite film is sufficiently lightly doped, it is possible that the perovskite layer can be completely depleted. Likewise, the PCBM ETL, which is reported in literature to be lightly n-doped, can also be fully depleted.[17] A typical measured $C–V$ curve for an optimized device is illustrated in **Figure 4**a. Qualitatively, the capacitance is flat at zero-bias and begins increasing only at forward bias voltages higher than 0.5 V. Furthermore, the $C–V$ curve at higher forward bias voltages is not entirely convex, as would be the case for a silicon device. These observations can be explained by the hypothesis that both the PCBM and the perovskite bulk are fully depleted at zero bias and the two regions of the curve, as illustrated in Figure 4a, correspond to the PCBM and perovskite depleting. This indicates that the perovskite film is also quite lightly doped.

We fabricate devices with varying perovskite film thicknesses and a constant PCBM thickness. At zero bias, the capacitance is flat for all thicknesses, indicating that the measured value is the combined capacitance of the perovskite and PCBM film in series. We plot the capacitance as a function of thickness (Figure 4b) and fit this curve using the capacitance of the PCBM layer and the dielectric constant of the perovskite film as fitting parameters. The details are provided in the Supporting Information. Based on the fitting we extract a value of 14.9 ± 5.3 for the relative dielectric constant of the perovskite film, which is reasonably consistent with prior reports.[18] The large error value reported here is mostly attributed to variations in the measured capacitance values and uncertainties in the thicknesses of the perovskite film. The $1/C^2–V$ plots for several different thicknesses of perovskite films are shown in Figure 4c. The plots show two distinct linear regions, corresponding to the PCBM and perovskite layer depleting. By fitting the linear portion and extrapolating, we can further estimate the built-in potential, which is about ≈0.93 eV for the 400 nm film. Evidently, the built-in potential is lower for thinner films, which agrees with the measured dark currents in these devices (Figure 4d). Because the measured doping level in the graphene is consistent, regardless of the perovskite thickness, it is likely that the reduced barrier height can be attributed to defects or trap states. From the electric constant and the built-in potential, we estimate that the doping of the perovskite film is $1.8 \times 10^{15}$ cm$^{-3}$ (see details in the Supporting Information). The light doping also explains the observation that the graphene remains heavily doped despite being in contact with

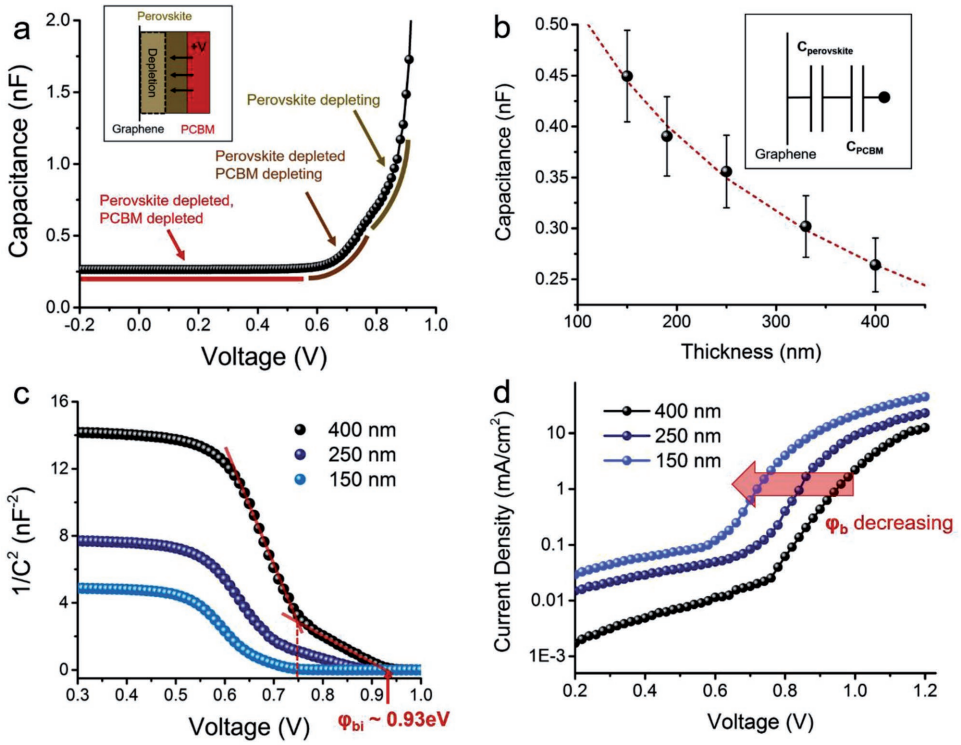


**Figure 4.** a) *C–V* measurements of graphene–perovskite solar cell. Inset: illustration of depletion. b) Total capacitance of perovskite film in series with PCBM film versus perovskite film thickness. Inset: illustration of series capacitance in this situation. c) $1/C^2$ plot of capacitance for devices of various thicknesses. Red lines are fitted to linear portions of plot. Built-in potential is estimated to be 0.93 eV. d) Dark current of corresponding devices.

an n-type semiconductor. We estimate that when the perovskite layer is fully depleted, the change in carrier concentration in the graphene necessary to maintain the built-in electric field is in the order of $10^{10}$ $cm^{-2}$ (see details in the Supporting Information), which is negligible compared to the measured doping level in graphene. Finally, if we take the effective density of states in the conduction band of the perovskite film to be $N_c = 4 \times 10^{19}$ $cm^{-3}$,[19] we can estimate that the Schottky barrier height is 1.19 eV, which is lower than the simplistic prior estimate from the difference in electron affinities (1.45 eV). This barrier height obtained from *C–V* measurements is also more consistent with the $V_{OC}$ values, which is typically a few hundred millivolts lower than the Schottky barrier height.

## 3. Conclusion

In conclusion, we fabricate graphene/perovskite Schottky barrier solar cells to investigate the excitonic versus free carrier models for perovskite solar cells. In order to uniformly deposit perovskite onto graphene and achieve an intimate interface between the perovskite and graphene, a variety of solution processing techniques are investigated. Device performances suggest that most photogenerated carriers in perovskite films are indeed dissociated, offering convincing evidence supporting the free carrier model. Furthermore, these devices have reasonable efficiencies of up to 10.6%. Devices without an ETL are also presented as a proof-of-concept demonstration. Although further work is necessary to prevent the perovskite and the metal cathode from reacting, we show that perovskite solar cells can function without a hole transport layer and an electron transport layer. Through *C–V* measurements, we also estimate the numerical values of some physical properties of perovskite films. This work represents an important advancement in understanding of perovskite solar cells and opens possibilities for alternative device designs in the future.

## 4. Experimental Section

*Graphene Synthesis and Transfer*: Single-layer graphene was synthesized on copper foil via low pressure chemical vapor deposition. Prior to growth, the copper foil (Alfa Aesar, 25 µm) was cleaned by sonicating in nickel etchant (Transene, type TFB) for 90 s and rinsing in deionized (DI) water. The as-grown graphene/copper was then coated with a 300 nm layer of poly(methyl methacrylate) (PMMA) and the copper was etched away using $FeCl_3$-based copper etchant (Transene). The floating graphene/PMMA was rinsed using DI water and scooped onto the glass substrate. After drying, the PMMA was removed by immersing in acetone at 80 °C.

*Device Fabrication*: PEDOT:PSS (Clevios PVP AI 4083) was filtered through a 0.45 µm syringe filter, spun onto ITO substrate at 4000 rpm for 30 s, and baked at 130 °C for 15 min. To coat PEDOT:PSS onto graphene, the filtered solution was mixed with surfactant (Triton X-100) 0.2 wt% and also spun at 4000 rpm. Lead acetate (Sigma-Aldrich) and methylammonium iodide (Sigma-Aldrich) were mixed in a 1:3 molar ratio and dissolved 43 wt% in DMF. Control devices (with PEDOT:PSS HTL) were fabricated by first preheating the substrate on a hot plate at 85 °C and dynamically spin-coating the precursor solution onto the PEDOT:PSS at 2000 rpm for 40 s. The substrate was immediately placed back onto the hot plate and baked at 85 °C for 15 min. Graphene–perovskite Schottky

devices were prepared by statically dispensing 70 µL of precursor solution onto a cold substrate and spinning at 2500 rpm for 90 s. To spin-coat onto graphene with the aid of additives, the as-prepared precursor solution was mixed with either 0.2 wt% surfactant or 0.5 wt% DiO and dynamically spin-coated at 2500 rpm for 90 s. After 3 min, the spin-coated films turn a light brown. The substrates are slowly heated to 85 °C by placing them onto the corner of the hot plate and pushing them toward the center, where they are left at 85 °C for 15 min. In all cases, the samples were then left in dry air for 4 h. $PC_{60}BM$ (1-material) was dissolved 35 mg $mL^{-1}$ in chlorobenzene and spin-coated onto the perovskite film at 1200 rpm for 30 s. The Ca/Al cathode (nominally 20 nm/80 nm) was thermally evaporated onto the PCBM through a shadow mask in high vacuum. For ETL-free devices, the metal was evaporated directly onto the perovskite film. The device active area is defined as the overlap area between the cathode and anode. Although the PEDOT:PSS layer and the PCBM layer cover the entire substrate, these layers are not sufficiently conductive to conduct carriers laterally. However, because this overlap area is not always constant, a metal aperture (50 nm Al) was thermally evaporated onto the back side of the device.

*Measurements and Characterization*: The sheet resistance and carrier concentration of the graphene films were measured using a home-built 4-point probe station. Cross-section SEM images were taken on devices physically cleaved using an FEI Helios 600. *I*/*V* curves were measured in a nitrogen glove box under AM1.5 illumination calibrated using a Newport 91150 V reference cell after light soaking for 5 min. A 50 nm thick aluminum layer was thermally evaporated onto the back-side of devices to serve as an aperture for measurements. Device area for ITO-based electrodes is nominally 5.4 $mm^2$ and device areas for graphene-based electrodes are nominally 1.6 $mm^2$; exact areas were measured under an optical microscope. Reported power conversion efficiencies and other performance parameters are based on the average and standard deviations of the 10 best devices of each type. EQE measurements were performed using chopped monochromatic light from a xenon lamp (Thermo Oriel 66921) through an optical fiber without bias illumination. *C*–*V* measurements were performed using an Agilent 4294A impedance analyzer with source frequency of 50 kHz.

## Acknowledgements

This work was sponsored by ENI Sp.A under the MITEI Solar Frontier Center. The authors would also like to thank D. Piedra for technical assistance in device measurements and Professor D. Antoniadis for use of measurement equipment.

## Conflict of Interest

The authors declare no conflict of interest.

## Keywords

graphene, perovskite, solar cells

Received: July 31, 2017
Revised: August 30, 2017
Published online: February 26, 2018

[1] A. Kojima, K. Teshima, Y. Shirai, T. Miyasaka, *J. Am. Chem. Soc.* **2009**, *131*, 6050.

[2] a) D. Y. Liu, T. L. Kelly, *Nat. Photonics* **2014**, *8*, 133; b) C. Tao, S. Neutzner, L. Colella, S. Marras, A. R. S. Kandada, M. Gandini, M. De Bastiani, G. Pace, L. Manna, M. Caironi, C. Bertarelli, A. Petrozza, *Energy Environ. Sci.* **2015**, *8*, 2365; c) W. Zhang, M. Saliba, D. T. Moore, S. K. Pathak, M. T. Horantner, T. Stergiopoulos, S. D. Stranks, G. E. Eperon, J. A. Alexander-Webber, A. Abate, A. Sadhanala, S. H. Yao, Y. L. Chen, R. H. Friend, L. A. Estroff, U. Wiesner, H. J. Snaith, *Nat. Commun.* **2015**, *6*, 6142; d) C. G. Wu, C. H. Chiang, Z. L. Tseng, M. K. Nazeeruddin, A. Hagfeldt, M. Gratzel, *Energy Environ. Sci.* **2015**, *8*, 2725.

[3] a) X. B. Xu, Q. Chen, Z. R. Hong, H. P. Zhou, Z. H. Liu, W. H. Chang, P. Y. Sun, H. J. Chen, N. De Marco, M. K. Wang, Y. Yang, *Nano Lett.* **2015**, *15*, 6514; b) L. K. Huang, Z. Y. Hu, J. Xu, X. X. Sun, Y. Y. Du, J. Ni, H. K. Cai, J. Li, J. J. Zhang, *Sol. Energy Mater. Sol. Cells* **2016**, *152*, 118; c) D. Y. Liu, J. L. Yang, T. L. Kelly, *J. Am. Chem. Soc.* **2014**, *136*, 17116; d) Y. Zhang, X. T. Hu, L. Chen, Z. Q. Huang, Q. X. Fu, Y. W. Liu, L. Zhang, Y. W. Chen, *Org. Electron.* **2016**, *30*, 281; e) K. W. Tsai, C. C. Chueh, S. T. Williams, T. C. Wen, A. K. Y. Jen, *J. Mater. Chem. A* **2015**, *3*, 9128.

[4] a) A. Miyata, A. Mitioglu, P. Plochocka, O. Portugall, J. T. W. Wang, S. D. Stranks, H. J. Snaith, R. J. Nicholas, *Nat. Phys.* **2015**, *11*, 582; b) K. Galkowski, A. Mitioglu, A. Miyata, P. Plochocka, O. Portugall, G. E. Eperon, J. T. W. Wang, T. Stergiopoulos, S. D. Stranks, H. J. Snaith, R. J. Nicholas, *Energy Environ. Sci.* **2016**, *9*, 962; c) V. D'Innocenzo, G. Grancini, M. J. P. Alcocer, A. R. S. Kandada, S. D. Stranks, M. M. Lee, G. Lanzani, H. J. Snaith, A. Petrozza, *Nat. Commun.* **2014**, *5*, 3586.

[5] W. G. Townsend, *IEEE J. Solid-State Electron Devices* **1978**, *2*, 31.

[6] W. Zhang, S. Pathak, N. Sakai, T. Stergiopoulos, P. K. Nayak, N. K. Noel, A. A. Haghighirad, V. M. Burlakov, D. W. deQuilettes, A. Sadhanala, W. Z. Li, L. D. Wang, D. S. Ginger, R. H. Friend, H. J. Snaith, *Nat. Commun.* **2015**, *6*, 10030.

[7] S. D. Stranks, G. E. Eperon, G. Grancini, C. Menelaou, M. J. P. Alcocer, T. Leijtens, L. M. Herz, A. Petrozza, H. J. Snaith, *Science* **2013**, *342*, 341.

[8] a) K. Domanski, J. P. Correa-Baena, N. Mine, M. K. Nazeeruddin, A. Abate, M. Saliba, W. Tress, A. Hagfeldt, M. Gratzel, *ACS Nano* **2016**, *10*, 6306; b) Y. Kato, L. K. Ono, M. V. Lee, S. H. Wang, S. R. Raga, Y. B. Qi, *Adv. Mater. Interfaces* **2015**, *2*, 1500195.

[9] a) P. You, Z. K. Liu, Q. D. Tai, S. H. Liu, F. Yan, *Adv. Mater.* **2015**, *27*, 3632; b) H. Sung, N. Ahn, M. S. Jang, J. K. Lee, H. Yoon, N. G. Park, M. Choi, *Adv. Energy Mater.* **2016**, *6*, 1501873.

[10] a) Y. M. Shi, K. K. Kim, A. Reina, M. Hofmann, L. J. Li, J. Kong, *ACS Nano* **2010**, *4*, 2689; b) J. K. Chang, W. H. Lin, J. I. Taur, T. H. Chen, G. K. Liao, T. W. Pi, M. H. Chen, C. I. Wu, *ACS Appl. Mater. Interfaces* **2015**, *7*, 17155; c) H. Park, J. A. Rowehl, K. K. Kim, V. Bulovic, J. Kong, *Nanotechnology* **2010**, *21*, 505204.

[11] a) X. Q. Li, W. C. Chen, S. J. Zhang, Z. Q. Wu, P. Wang, Z. J. Xu, H. S. Chen, W. Y. Yin, H. K. Zhong, S. S. Lin, *Nano Energy* **2015**, *16*, 310; b) Y. Song, X. M. Li, C. Mackin, X. Zhang, W. J. Fang, T. Palacios, H. W. Zhu, J. Kong, *Nano Lett.* **2015**, *15*, 2104.

[12] K. Yan, Z. Wei, J. Li, H. Chen, Y. Yi, X. Zheng, X. Long, Z. Wang, J. Wang, J. Xu, S. Yang, *Small* **2015**, *11*, 2269.

[13] S. Lee, J. S. Yeo, Y. Ji, C. Cho, D. Y. Kim, S. I. Na, B. H. Lee, T. Lee, *Nanotechnology* **2012**, *23*, 344013.

[14] a) P. W. Liang, C. Y. Liao, C. C. Chueh, F. Zuo, S. T. Williams, X. K. Xin, J. J. Lin, A. K. Y. Jen, *Adv. Mater.* **2014**, *26*, 3748; b) J. Kniepert, I. Lange, J. Heidbrink, J. Kurpiers, T. J. K. Brenner, L. J. A. Koster, D. Neher, *J. Phys. Chem. C* **2015**, *119*, 8310.

[15] H. C. Liao, C. C. Ho, C. Y. Chang, M. H. Jao, S. B. Darling, W. F. Su, *Mater. Today* **2013**, *16*, 326.

[16] Y. Song, W. J. Fang, A. L. Hsu, J. Kong, *Nanotechnology* **2014**, *25*, 395701.

[17] B. Ecker, J. C. Nolasco, J. Pallares, L. F. Marsal, J. Posdorfer, J. Parisi, E. von Hauff, *Adv. Funct. Mater.* **2011**, *21*, 2705.

[18] M. Samiee, S. Konduri, B. Ganapathy, R. Kottokkaran, H. A. Abbas, A. Kitahara, P. Joshi, L. Zhang, M. Noack, V. Dalal, *Appl. Phys. Lett.* **2014**, *105*, 153502.

[19] Y. C. Zhou, A. Gray-Weale, *Phys. Chem. Chem. Phys.* **2016**, *18*, 4476.